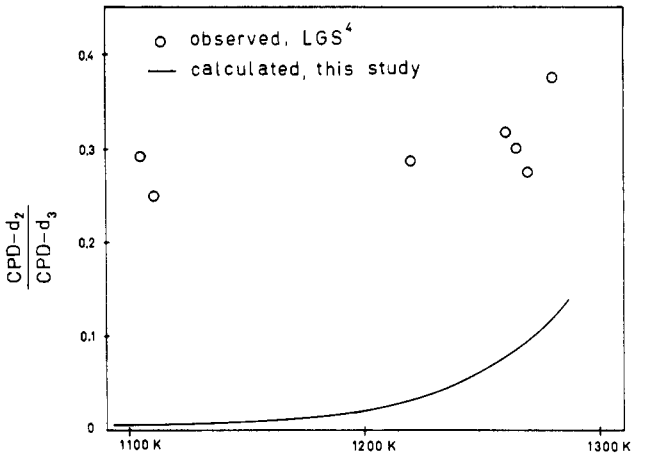

Figure 3. Calculated vs experimental ratios of CPD-d_2 to CPD-d_3, produced from CP-*3,3,4,4-*d_4 after 800-μs reaction time. For rate constants used in the model, see Figure 1 and text.

one-third of the observed CPD-d_2 can be attributed to the degenerate isomerization via VCP. At 1100 K, the calculated amount of CPD-d_2 is lower than the experimentally observed quantity by more than a factor of 20.

Discussion

The new experimental data on the CP → VCP reaction and the calculations described in the preceding section indicate that the extent of isomerization of CP-*3,3,4,4-*d_4 to CP-*3,3,5,5-*d_4 within 8×10^{-4} s is very small below 1200 K but that it begins to rise rapidly at higher temperatures, especially above 1250 K. Thus, the expected ratio of the CPD's produced by *3,5* molecular hydrogen elimination from nascent CP-*3,3,5,5-*d_4 and the residual CP-*3,3,4,4-*d_4 would be expected to rise very rapidly with temperature, especially at the high end of the 1100–1280 K range explored by LGS.[4] The experiments of LGS, however, showed only a small temperature dependence. The highest temperature experiment, at 1280 K, gave a mass 68/69 CPD ratio that was 0.1 higher than the other data points (0.4 vs about 0.3), and this may represent the small but significant influence of CP degenerate isomerization via VCP at that temperature.

In order for isomerization of deuterated CP, before exclusive 3,5 hydrogen elimination, to account for the observed mass 68/69 CPD ratios, the isomerization process would have to approach equilibrium within the 8.0×10^{-4} s reaction time at any temperature above 1100 K. Intramolecular isomerization of CP via VCP occurs too slowly to achieve equilibration of the label at positions 3, 4, and 5, at temperatures below 1300 K. Some other process, in addition to cis 3,5 molecular hydrogen elimination, must be invoked to explain the mass 68/69 product ratios and the apparent D_2 elimination from cyclopentene-*3,3,4,4-*d_4, observed by LGS.

Acknowledgment. This study was supported by National Science Foundation Grant CHE-8721656 and by a William and Flora Hewlett Foundation grant of Research Corporation.

Registry No. Cyclopentene, 142-29-0.

Ab Initio Study of the Reactions between Methane and OH, H, and ^3O

C. Gonzalez, J. J. W. McDouall,† and H. B. Schlegel*

Department of Chemistry, Wayne State University, Detroit, Michigan 48202 *(Received: August 22, 1989; In Final Form: April 9, 1990)*

The primary processes in methane combustion include hydrogen abstraction by radicals to form CH_3. Ab initio molecular orbital calculations have been used to study three important reactions contributing to the formation of the methyl radical: $CH_4 + X \rightarrow CH_3 + HX$, where X = OH, H, and ^3O. Optimized geometries and harmonic vibrational frequencies have been calculated for all reactants, transition states, and products at the HF/6-31G** and UMP2/6-31G** levels. Barriers and heats of reaction have been estimated by fourth-order Møller–Plesset perturbation theory with spin projection (PMP4(SDTQ)) using the 6-311G** basis set. Nonvariational transition-state theory has been used to treat the kinetics of these reactions; even without any scaling of parameters, the temperature dependence of the rate constants shows reasonably good agreement with experiment.

Introduction

The mechanism of the combustion of C_1 and C_2 hydrocarbons has been studied extensively.[1,2] In general, hydrocarbons can react with a variety of radicals produced in flames to generate a significant concentration of CH_3, which is oxidized to CO and CO_2 in subsequent steps (under stoichiometric conditions and lean flames):

$$CH_4 \xrightarrow{OH,\ H,\ ^3O} CH_3 \xrightarrow{^3O} CH_2O \xrightarrow{OH,\ H,\ ^3O} CHO \xrightarrow{M,\ O_2,\ H} CO \rightarrow CO_2 \quad (1)$$

The initial attack of methane by OH, H, and ^3O proceeds by

$$CH_4 + OH \rightarrow CH_3 + H_2O \quad (2)$$

$$CH_4 + H \rightarrow CH_3 + H_2 \quad (3)$$

$$CH_4 + {}^3O \rightarrow CH_3 + OH \quad (4)$$

Reactions 2–4 have been studied experimentally, and their rate coefficients have been determined in the temperature range 300–2500 K.[3-5] Ab initio studies of the reactions of $CH_4 + H$ and $CH_4 + OH$ have been performed at the UHF/6-31G level by Leroy et al.,[6] and the corresponding reaction rate coefficients (calculated by the nonvariational transition-state theory formalism) were obtained by using a semiempirical model where the CH_3–H and the H–X (X = H, OH) bonds are treated as Morse oscillators. In addition, molecular orbital calculations using POL-CI wave

† Present address: Department of Chemistry, University of Manchester, Manchester M13 9PL, U.K.

(1) Hucknall, D. J. *Chemistry of Hydrocarbons*; Chapman and Hall: London, 1985; p 74.
(2) Warnatz, J. In *Combustion Chemistry*; Gardiner, W. C., Jr., Ed.; Springer-Verlag, New York, 1984; p 233 and references therein.
(3) Ernst, J.; Wagner, H.; Zellner, R. *Ber. Bunsen-Ges. Phys. Chem.* **1978**, *82*, 409.
(4) Clark, T. C.; Dove, J. E. *Can. J. Chem.* **1973**, *51*, 2147. Clark, T.; Dove, J. E. *Can. J. Chem.* **1973**, *51*, 2155. Roth, P.; Just, Th. *Ber. Bunsen-Ges. Phys. Chem.* **1975**, *79*, 682.
(5) Roth, P.; Just, Th. *Ber. Bunsen-Ges. Phys. Chem.* **1977**, *81*, 572. Klemm, R. B.; et al. *18th Symposium (International) on Combustion*; 1981; p 785.
(6) Leroy, G.; Sana, M.; Tinant, A. *Can. J. Chem.* **1985**, *63*, 1447.

0022-3654/90/2094-7467$02.50/0

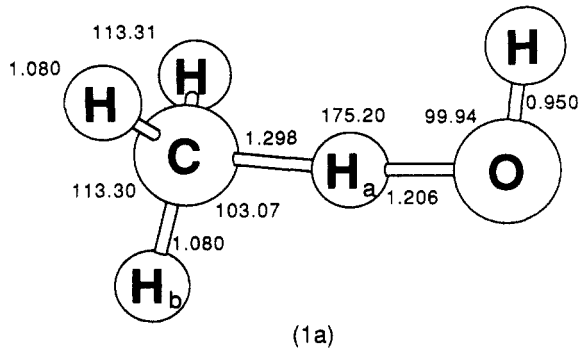

(1a)

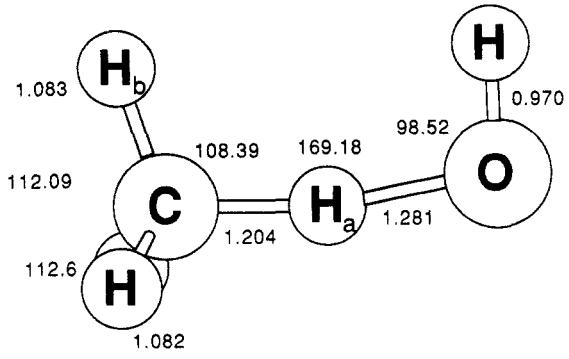

(1b)

Figure 1. Transition structure for $CH_4 + OH \rightarrow CH_3 + H_2O$. (a) HF/6-31G** optimized, (b) UMP2/6-31G** optimized.

functions have been carried out to determine the barriers for the hydrogen-abstraction reactions of $CH_4 + H$ and $CH_4 + {}^3O$.[7-10] Previous studies have shown that the transition structures calculated at the UHF level are affected by a considerable amount of spin contamination,[11-13] and as a result, the reaction barriers can be overestimated by up to 10 kcal/mol when correlation corrections are calculated by Møller–Plesset perturbation theory.

In the present work, spin projection and Møller–Plesset perturbation theory are employed to obtain the barriers and energetics of reactions 2–4. The calculated barriers are used in conjunction with nonvariational transition-state theory to determine the corresponding rate constants in the temperature range 300–1000 K. The results are compared with experiment.

Method

Ab initio molecular orbital calculations were performed by using the GAUSSIAN 88 system of programs.[14] Fully optimized geometries, harmonic vibrational frequencies, and zero-point energies of the reactants, transition structures, and products were calculated at the Hartree–Fock and UMP2 levels by using the 6-31G** basis set[15] with analytical derivatives.[16] Electron correlation was calculated with the fourth-order Møller–Plesset perturbation theory in the space of single, double, triple, and quadruple excitations with annihilation of spin contamination from $s + 1$ to $s + 4$[13,17,18] with the 6-311G** basis set[19] using the optimized geometries obtained at the UMP2/6-31G** level (PMP4SDTQ/6-311G**//UMP2/6-31G**).

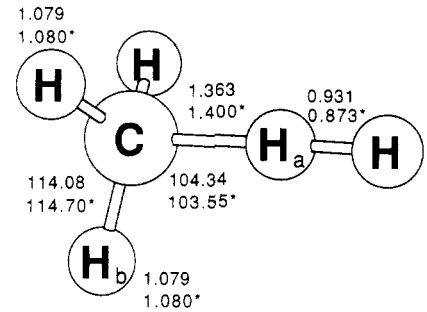

Figure 2. Transition structure for $CH_4 + H \rightarrow CH_3 + H_2$ (no superscript, HF/6-31G** optimized; asterisk, UMP2/6-31G** optimized).

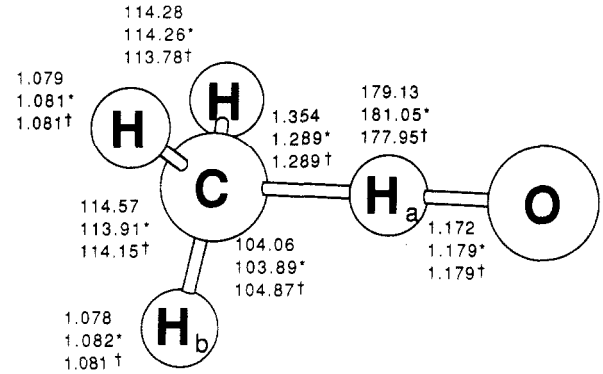

Figure 3. Transition structure for $CH_4 + {}^3O \rightarrow CH_3 + OH$ (no superscript, HF/6-31G** optimized; asterisk, UMP2/6-31G**-optimized geometry for the $^3A'$ state; dagger, UMP2/6-31G**-optimized geometry for the $^3A''$ state).

TABLE I: Total Energies for Reactants, Transition Structures, and Products for $CH_4 + X \rightarrow CH_3 + HX$ (X = OH, H, and ^3O)[a]

reaction	reactants	transition state	products
$CH_4 + OH$	−115.993 172	−115.976 640	−116.007 067
	−115.994 005	−115.979 591	−116.008 209
$CH_4 + H$	−40.904 653	−40.877 049	−40.899 445
	−40.904 653	−40.879 893	−40.899 445
$CH_4 + {}^3O\ (^3A')$	−115.338 170	−115.304 968	−115.320 914
	−115.338 845	−115.308 377	−115.320 914
$CH_4 + {}^3O\ (^3A'')$	−115.338 170	−115.304 973	−115.320 914
	−115.338 845	−115.308 383	−115.320 914

[a] Total energies in au calculated at the MP4(SDTQ)/6-311G** level using geometries optimized at the UMP2/6-31G** level. For each reaction, the first line is without spin projection (UMP4) and the second line is with spin projection (PMP4). $\langle s^2 \rangle - s(s+1) =$ 0.00069–0.00730 for reactants and products and 0.00990–0.01580 for the transition states.

The rate constants were calculated by using the nonvariational transition-state theory formalism, including Wigner's tunneling correction $\Gamma(T)$:[20]

$$k_r(T) = \Gamma(T)\frac{k_b T}{h}\frac{Q^*(T)}{Q_{CH_4}(T)Q_X(T)}\exp\left(\frac{-\Delta E^*}{k_b T}\right) \quad (5)$$

with

$$\Gamma(T) = 1 + \frac{1}{24}\left(\frac{h|\nu^*|}{k_b T}\right)^2 \quad (6)$$

where $Q^*(T)$, $Q_{CH_4}(T)$, and $Q_X(T)$ are the total partition functions for the transition state, methane, and X = OH, H, or ^3O at temperature T, ΔE^* is the activation energy (including

(7) Walch, S. P. *J. Chem. Phys.* **1980**, *72*, 4932.
(8) Schatz, G. C.; Walch, S. P.; Wagner, A. F. *J. Chem. Phys.* **1980**, *73*, 4536.
(9) Walch, S. P.; Dunning, T. H., Jr. *J. Chem. Phys.* **1980**, *72*, 3221.
(10) Schatz, G. C.; Wagner, A. F.; Dunning, T. H. *J. Phys. Chem.* **1984**, *88*, 221.
(11) Sosa, C.; Schlegel, H. B. *Int. J. Quantum Chem.* **1986**, *29*, 1001; **1987**, *30*, 155.
(12) Sosa, C.; Schlegel, H. B. *Int. J. Quantum Chem. Symp.* **1987**, *21*, 267.
(13) Gonzalez, C.; Sosa, C.; Schlegel, H. B. *J. Phys. Chem.* **1989**, *93*, 2435.
(14) Frish, M. J.; Head-Gordon, M.; Schlegel, H. B.; Raghavachari, K.; Binkley, J. S.; Gonzalez, C.; Defrees, D. J.; Fox, D. J.; Whiteside, R. A.; Seeger, R.; Melius, C. F.; Baker, J.; Martin, R.; Kahn, L. R.; Stewart, J. J. P.; Fluder, E. M.; Topiol, S.; Pople, J. A. *Gaussian 88*; Gaussian, Inc.: Pittsburgh, PA, 1988.
(15) Hariharan, P. C.; Pople, J. A. *Chem. Phys. Lett.* **1972**, *66*, 217.
(16) Schlegel, H. B. *J. Comput. Chem.* **1982**, *3*, 214.
(17) Schlegel, H. B. *J. Chem. Phys.* **1986**, *84*, 4530.
(18) Schlegel, H. B. *J. Phys. Chem.* **1988**, *92*, 3075.
(19) Krishnan, R.; Binkley, J. S.; Pople, J. A. *J. Chem. Phys.* **1980**, *72*, 650.
(20) Wigner, E. P. *Z. Phys. Chem.* **1932**, *B19*, 203.

TABLE II: Barrier Heights, Zero-Point Energy (ZPE) Corrections, and Vibrational Adiabatic Barriers (VAB) for $CH_4 + X \rightarrow CH_3 + HX$ (X = OH, H, and ^3O)

reaction	barrier height[a]	ΔZPE	VAB[b]
	Without Spin Projection		
$CH_4 + OH$	10.37	−1.71	8.66
$CH_4 + H$	17.32	−1.33	15.99
$CH_4 + {}^3O\ (^3A')$	20.83	−3.78	17.05
$CH_4 + {}^3O\ (^3A'')$	20.84	−3.77	17.07
	With Spin Projection		
$CH_4 + OH$	9.05	−1.71	7.34
$CH_4 + H$	15.53	−1.33	14.20
$CH_4 + {}^3O\ (^3A')$	19.12	−3.78	15.34
$CH_4 + {}^3O\ (^3A'')$	19.12	−3.77	15.35

[a] Barriers in kcal/mol calculated at the MP4(SDTQ)/6-311G** level using geometries optimized at the UMP2/6-31G** level. [b] VAB = barrier height + ΔZPE.

TABLE III: Vibrational Frequencies for Minima and Transition Structures for $CH_4 + X \rightarrow CH_3 + HX$ (X = OH, H, and ^3O)[a]

molecule	frequencies, cm^{-1}
	Minima
CH_4	1407, 1407, 1407, 1627, 1627, 3135, 3283, 3283, 3283
H_2	4611
OH	3845
CH_3	395, 1491, 1491, 3243, 3441, 3441
H_2O	1684, 3895, 4033
	Transition Structures
CH_3--H--OH	2055*i*, 44, 291, 356, 745, 941, 1208, 1327, 1465, 1522, 1545, 3177, 3317, 3323, 3845
CH_3--H--H	1744*i*, 571, 572, 1136, 1202, 1202, 1505, 1505, 1933, 3190, 3355, 3356
CH_3--H--^3O ($^3A'$)	2197*i*, 313, 421, 609, 1081, 1236, 1276, 1501, 1505, 3183, 3340, 3341
CH_3--H--^3O ($^3A''$)	2198*i*, 325, 423, 610, 1082, 1233, 1276, 1502, 1505, 3182, 3340, 3344

[a] Frequencies calculated at the UMP2/6-31G** level.

thermal corrections to the internal energy and zero-point energy), ν^* is the imaginary frequency at the transition state, k_b is Boltzmann's constant, and h is Planck's constant. In general, the Wigner tunneling correction is only a crude model. However, since a high degree of accuracy is not intended, its use seems to be adequate for the purpose of this paper. In addition, previous studies conducted by Truhlar on the dynamics of the reaction of $CH_3 + H_2$ indicate agreement with the experimental rates within a factor of 2.5 when Wigner tunneling corrections are used.[21] If better agreement is desired, more sophisticated methods such as the small curvature approximation[22] are necessary. In this case, detailed knowledge of the reaction path is needed.

Results and Discussion

Figures 1–3 show the optimized geometries of the transition structures for the three reactions under study. Table I lists the total energies for reactants, transition structures, and products calculated at the PMP4(SDTQ)/6-311G** level using the optimized geometries from the UMP2/6-31G** level, while Table II shows the barrier heights, the zero-point energies (calculated by using harmonic vibrational frequencies at the UMP2/6-31G** level), and the vibrationally adiabatic barriers. The harmonic vibrational frequencies calculated at the UMP2/6-31G** level are collected in Table III. In general, the harmonic vibrational frequencies at the MP2/6-31G** level are approximately 6% higher than the experimental values, primarily due to basis set effects and neglect of anharmonicity.[27]

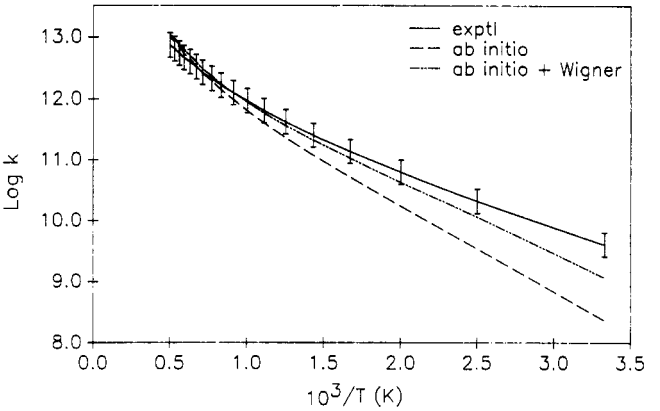

Figure 4. Arrhenius plot for $CH_4 + OH \rightarrow CH_3 + OH$. Inclusion of Wigner tunneling corrections (dash–dot curve) results in a better agreement with experimental rate constants (solid curve).

Transition Structures. In all three cases, the methyl fragment shows a considerable degree of pyramidalization, which is consistent with the fact that the out-of-plane bending potential for the methyl radical is broad and shallow.[24] Progress along the reaction coordinate can be judged by comparing the C–H_a bond lengths in the transition state: $CH_4 + OH$ is the earliest (R = 1.204 Å), $CH_4 + {}^3O$ is intermediate (R = 1.289 Å), and $CH_4 + H$ is the latest (R = 1.400 Å). Since $CH_4 + {}^3O$ is more endothermic than $CH_4 + H$, one might have expected the order of the last two reactions to be reversed, based on Hammond's postulate. For $CH_4 + {}^3O$, there are two surfaces that must be considered separately: the $^3A'$ state with the half-filled p orbital in the H_bCO plane and the $^3A''$ state with the half-filled p orbital perpendicular to the plane. The two transition states are almost identical in energy but differ slightly in the OHC bending angle (181° for $^3A'$ and 178° for $^3A''$) and the tilt of the methyl group (as shown in Figure 3).

For the reaction of $CH_4 + OH$, the C–H_a bond is longer than the O–H_a bond at the Hartree–Fock level (1.298 Å vs 1.206 Å; see figure 1a) but the situation is reversed at the UMP2 level (1.204 Å vs 1.281 Å; see Figure 1b). Furthermore, the transition structure at the Hartree–Fock level is such that the OH fragment is trans with respect to one of the C–H bonds of the methyl group whereas the UMP2 transition structure is cis (the trans conformer is a second-order saddle point).

Both the HF/6-31G** and the UMP2/6-31G** levels were used to compute the vibrational frequencies and zero-point energies. On average, the UMP2 frequencies are 6% lower than the Hartree–Fock values. In contrast to the small and systematic changes in the frequencies for the stable vibrational modes, there are large changes in the imaginary frequencies that correspond to motion along the transition vector. The UMP2/6-31G** values are $600i$–$1000i$ cm^{-1} smaller than the Hartree–Fock values. In the low-temperature region, this reduces the Wigner tunneling correction by almost a factor of 2.

Barrier Heights. The calculated barrier for hydrogen abstraction by OH is 7.34 kcal/mol (PMP4/6-311G**//UMP2/6-31G** with ZPE), which is within the experimental range of 4–7 kcal/mol.[2] In $CH_4 + H$, the calculated barrier, 14.20 kcal/mol, is in good agreement with the value of 13.5 kcal/mol obtained by Walch[7] using the POL-CI method. However, both

(21) Steckler, R.; Dykema, K. J.; Brown, F. B.; Hancock, G. C.; Truhlar, D. G.; Valencich, T. J. *J. Chem. Phys.* **1987**, *87*, 7024.
(22) Skodje, R. T.; Truhlar, D. G.; Garret, B. C. *J. Chem. Phys.* **1982**, *77*, 5955.
(23) Baldridge, K. K.; Gordon, M. S.; Steckler, R.; Truhlar, D. G., submitted for publication to *J. Phys. Chem.*
(24) Yamada, C.; Hirota, E.; Kawaguchi, K. J. *J. Chem. Phys.* **1981**, *75*, 5256. Riveros, J. M. *Chem. Phys.* **1969**, *51*, 1269. Chipman, D. M. *J. Chem. Phys.* **1983**, *78*, 3112.
(25) Benson, S. W. *Thermochemical Kinetics*, 2nd ed.; Wiley: New York, 1976.
(26) Herschbach, D. R.; Johnston, H. S.; Pitzer, K. S.; Powell, R. F. *J. Chem. Phys.* **1956**, *25*, 736.
(27) Guo, H.; Karplus, M. *J. Chem. Phys.* **1989**, *91*, 1719. Simandiras, E. D.; Amos, R. D.; Handy, N. C.; Lee, T. J.; Rice, J. E.; Remington, R. B.; Schaefer, H. F. *J. Am. Chem. Soc.* **1988**, *110*, 1388. Fogarasi, G.; Pulay, P. *Ann. Rev. Phys. Chem.* **1984**, *35*, 191. Fogarasi, G.; Pulay, P. In *Vibrational Spectra and Structure*; Durig, J. R., Ed.; Elsevier: Amsterdam, 1985; Vol. 14.

TABLE IV: Summary of Thermodynamic Analysis and Arrhenius Parameters for Temperatures 300, 1000, and 2000 K[a-c]

T, K	$\Delta E^{\ddagger}$	$\Delta H^{\ddagger}$	E_a[d]	ΔH_{rxn}	Wigner[e]	log k	log k(exp)[f]	A(calc)
				$CH_4 + OH \rightarrow CH_3 + H_2O$				
300	6.38	5.78	6.97	-10.60	5.05	9.07	9.70	1.31×10^{14}
1000	7.61	5.62	9.59	-11.32	1.36	11.95	12.02	1.07×10^{14}
2000	9.53	5.56	13.51	-14.17	1.09	13.04	12.98	3.24×10^{14}
				$CH_4 + H \rightarrow CH_3 + H_2$				
300	13.56	12.96	14.16	0.11	3.91	4.44	5.40	3.94×10^{14}
1000	14.60	12.62	16.59	-0.41	1.26	10.94	11.43	7.87×10^{14}
2000	16.33	12.36	20.31	-3.98	1.07	12.69	13.29	2.08×10^{15}
				$CH_4 + {}^3O \rightarrow CH_3 + OH$				
300	10.31	9.72	10.91	8.79	5.63	6.77	6.73	2.61×10^{14}
1000	12.35	10.36	14.34	6.50	1.42	11.48	11.43	1.14×10^{15}
2000	14.59	10.62	18.57	3.16	1.10	13.18	13.18	4.44×10^{15}

[a] Except for log k(exp), all values were calculated in this work. [b] All the energies and heats of reaction in kcal/mol. [c] Arrhenius A factors and reaction rates coefficients k in $cm^3/(mol \cdot s)$. [d] $E_a = RT(\ln(A) - RT \ln(k))$. [e] Wigner tunneling correction, eq 6. [f] Reference 2.

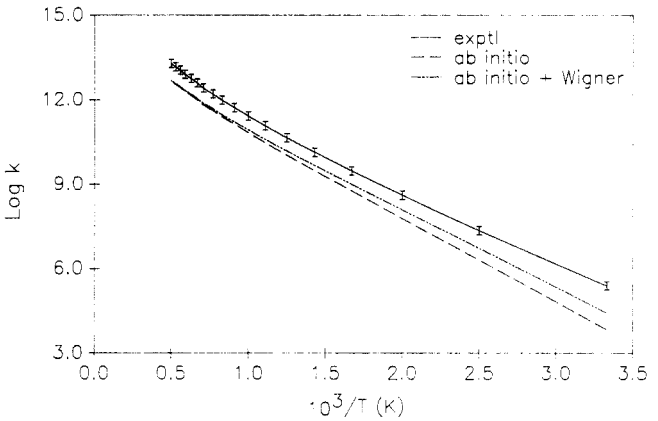

Figure 5. Arrhenius plot for $CH_4 + H \rightarrow CH_3 + H_2$. Even though the agreement between the calculated and experimental rate constants improves when Wigner tunneling corrections are included (dash-dot curve), the results are consistently lower than the experimental values (solid curve), probably due to overestimation of the barrier.

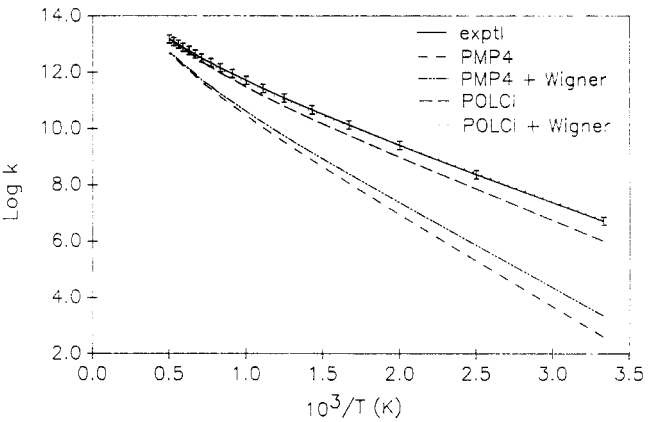

Figure 6. Arrhenius plot for $CH_4 + {}^3O \rightarrow CH_3 + OH$. Single reference MP4 calculations overestimate the reaction barrier, producing very low reaction rates (medium dash and dash-dot curves) when compared with the experimental results (solid curve). When the rate constants are recalculated with the POL-CI barrier and UMP2/6-31G** frequencies and partition functions, the agreement with the experiment is excellent (long dash and dotted curves).

are somewhat higher than the values obtained experimentally, 11–12 kcal/mol.[2] Likewise, for the case of $CH_4 + {}^3O$, the calculated barrier, 15.34 kcal/mol, is approximately 4 kcal/mol higher than the experimental barrier of 9.0–11.4 kcal/mol.[2] The calculated difference in the barrier heights on the $^3A''$ and $^3A'$ surfaces (with ZPE corrections included) is only 0.01 kcal/mol. In a large POL-CI(SOGVB) calculation with a [3s2p1d/2s1p] basis, Walch and Dunning[9] have obtained a barrier 5 kcal/mol lower (10.3 kcal/mol for the $^3A'$ surface and 10.1 kcal/mol for the $^3A''$ surface), suggesting that this reaction requires a multiconfigurational reference space. Spin projection at the PMP4 level lowers the calculated barriers by ca. 1.3–1.8 kcal/mol (Table II).

Reaction Rates. Nonvariational transition-state theory (TST) calculations in the temperature range 300–2000 K were performed for reactions 2–4 using eqs 5 and 6. In the case of $CH_4 + {}^3O$, the reaction rate constants were calculated separately for the $^3A'$ and $^3A''$ surfaces and added to obtain the total rate constant. The results of these calculations are shown graphically in Figures 4–6; the experimental curves as recommended by Warnatz[2] are also shown for the purpose of comparison. In addition, a summary of the TST calculations for three different temperatures (300, 1000, and 2000 K) is given in Table IV.

$CH_4 + OH$. The transition state for this reaction exhibits a very low frequency mode (ca. 44 cm^{-1}). Since this mode corresponds to the rotation of the OH fragment around the partially formed OH_a bond (Figure 1b), it was treated as an internal rotor rather than a vibrator. This approximation seems reasonably valid in the present case due to the almost negligible rotational barrier of the OH fragment. The partition function for the internal rotor is[25]

$$Q_{ir} = (8\pi^3 I_r k_b T)^{1/2}/\sigma h = 0.35(I_r T)^{1/2}/\sigma \qquad (7)$$

where k_b and h are Boltzmann's and Planck's constants respectively, T is the temperature in K, σ is the symmetry number of the internal rotation, and I_r is the reduced moment of inertia in amu·Å^2 (calculated by the method of Herschbach et al.[26]).

As can be observed in Figure 4, the calculated rates are systematically lower than the experimental ones. The difference is more pronounced in the low-temperature region where tunneling effects are significant. The inclusion of the Wigner tunneling correction improves substantially the agreement with the experimental fit. The curvature of the plot is reproduced, but the individual values of the rate constants are somewhat lower than the experiment, especially at low temperatures ($T < 400$ K). The difference between these values could be attributed to overestimation of the reaction barrier, lack of cancellation of anharmonicity corrections between transition state and reactants, or recrossing effects.

$CH_4 + H$. Figure 5 shows a plot of log k_r vs $1/T$ for abstraction by H atom. The calculated rate constants with and without Wigner tunneling corrections are consistently lower than the experimental results. This can be traced to the difference in the calculated and experimental barrier heights (14.20 kcal/mol vs 11–12 kcal/mol). Nevertheless, there is good agreement with experiment in terms of the shape of the Arrhenius plot in the whole temperature range.

$CH_4 + {}^3O$. The Arrhenius-type plot for this reaction is shown in Figure 6. The results obtained at the PMP4(SDTQ) level of theory are in poor agreement with the experimental values even after applying the Wigner tunneling correction. Although a reasonably large basis set has been used, it appears that the single reference MP4 calculations may not be able to reproduce the correct barrier for this reaction. In order to overcome this problem, the reaction rate constants were recalculated with the barrier

height obtained in a POL-CI calculation by Walch and Dunning[7] along with the frequencies, partition functions, and zero-point energies from the present calculations. As shown in Figure 6, the rate constants calculated in this manner and corrected by tunneling effects are in excellent agreement with the experimental results.

General Features. Even though the three reactions exhibit similar curvature in the temperature dependence of their reaction rate constants, there are significant differences. In the case of CH_4 + OH, Arrhenius behavior is observed at temperatures lower than 900 K. However, above 900 K, the plot is not linear. Less deviation from linearity is observed in the reactions of CH_4 + H and CH_4 + ^3O (see Figures 2-4). The pronounced nonlinearity observed above 900 K in the Arrhenius plot for the reaction of CH_4 + OH could be because the vibrational partition function, Q_{vib}^*, becomes too large at higher temperatures due to the low frequency modes in the transition state. The reaction of CH_4 + OH is faster than the other two over the whole temperature range (see Figures 2-4 and Table IV) despite the fact that the A factors are quite similar. This is expected from the lower barrier for CH_4 + OH (see Table II). This conclusion is supported by the results reported in Table IV, where the activation energies E_a for this reaction are consistently lower than the corresponding values for the reactions of CH_4 + H, OH. Furthermore, the abstraction reaction by OH is exothermic in the whole temperature range, while the reaction with H becomes exothermic only at high temperatures. The reaction of CH_4 + ^3O is found to be endothermic for all the temperatures studied in this work.

Conclusions

Ab initio calculations at the PMP4(SDTQ)/6-311G** level have been used to study the hydrogen-abstraction reaction between methane and OH, H, and ^3O. The comparison between the reaction rate constants calculated with the transition-state theory and the experimental results indicate a good agreement in the case of CH_4 + OH and CH_4 + H. The same comparison for CH_4 + ^3O shows that single reference MP4 calculations overestimate the barrier height, producing too low a reaction rate constant when compared with the experiment. The situation is corrected when a POL-CI barrier is used together with the frequencies and partition functions calculated at the UMP2/6-31G** level. Spin projection lowers the barrier heights by ca. 1-2 kcal/mol, indicating the importance of removing the unwanted spin states from the UHF wave functions. The simple studies conducted in this work indicate that the direct dynamics approach advocated by Truhlar[23] can yield useful data on these important reactions, providing a qualitative description of the temperature dependence of the reaction rate constants.

Acknowledgment. We thank Prof. William Hase for interesting and helpful discussions. This work was supported by a grant from the National Science Foundation (CHE-87-11901) and by the Pittsburgh Supercomputer Center.

Registry No. CH_4, 74-82-8; OH, 3352-57-6; H, 12385-13-6; ^3O, 17778-80-2.

Rotating Ring Disk Electrode Theory Dealing with Nonstationary Electrocatalysis: Study of the Electrocatalytic Reduction of Dioxygen at Cobalt Protoporphyrin Modified Electrode

Rongzhong Jiang and Shaojun Dong*

Changchun Institute of Applied Chemistry, Academia Sinica, Changchun, Jilin 130022, People's Republic of China *(Received: August 22, 1989; In Final Form: April 13, 1990)*

An equation describing the variation of rate constant (k) with reaction charge (Q) and potential (E) for electrocatalysis is derived. A rotating ring disk electrode (RRDE) theory dealing with kinetic problems for dioxygen reduction at an unstable electrode is proposed. Using a rotation-scan RRDE method the kinetic behavior for the catalytic reduction of dioxygen at cobalt protoporphyrin modified pyrolytic graphite (CoPP/PG) was investigated. Even if several variable factors exist simultaneously, such as the activity of ring and disk electrodes, as well as the concentration of dioxygen in solution, the variation of rate constants with Q and E values for dioxygen reduction at CoPP/PG electrode can be calculated successfully. An equation involving the variables of k, Q, and E was obtained experimentally, and it can be used to describe electrode activity and stability for the catalytic reduction of dioxygen.

Introduction

Generally, most electrocatalytic systems are not very stable. For example, no absolutely stable catalyst and electrode for dioxygen reduction have so far been found.[1-3] The electrocatalytic reduction of dioxygen at transition-metal porphyrins and phthalocyanines is a problem that has received attention.[4-11] Recently, highly active dicobalt porphyrin has been synthesized by Collman and Anson et al.,[4] which can catalyze dioxygen four-electron reduction to water. Unfortunately, the catalytic activity of these porphyrin and phthalocyanines is neither durable nor stable for dioxygen reduction. Instability has made measurement of kinetic data difficult. The rotating disk or ring disk electrode (RDE or RRDE) is a useful tool for investigating catalytic kinetic process.[12-16] When this method is used to study catalytic reduction of dioxygen, some unstable factors may arise, including the ring and disk activity, concentration of O_2 in solution, so that intermediate product (H_2O_2) concentration for dioxygen

* To whom correspondence should be addressed.

(1) Yeager, E. *J. Electrochem. Soc.* **1981**, *128*, 160C.
(2) Yeager, E. *Electrochim. Acta* **1984**, *29*, 1527.
(3) van den Brink, F.; Barendrecht, E.; Visscher, W. *Recl: J. R. Neth. Chem. Soc.* **1980**, *99*, 253.
(4) Colman, J. P.; Denisevich, P.; Konai, Y.; Marrocco, M.; Koval, C.; Anson, F. C. *J. Am. Chem. Soc.* **1980**, *102*, 6027.
(5) Duran, R. R.; Anson, F. C. *J. Electroanal. Chem.* **1982**, *134*, 273.
(6) Bettelheim, A.; Kuwana, T. *Anal. Chem.* **1979**, *51*, 2257.
(7) Liu, H. Y.; Abdalmuhdi, I.; Chang, C. K.; Anson, F. C. *J. Phys. Chem.* **1985**, *89*, 665.
(8) Jiang, R.; Dong, S. *J. Electroanal. Chem.* **1988**, *246*, 101.
(9) Dong, S.; Jiang, R. *J. Inorg. Biochem.* **1987**, *30*, 189.
(10) Dong, S.; Jiang, R. *J. Mol. Catal.* **1987**, *42*, 37.
(11) Dong, S.; Jiang, R. *Ber. Bunsen-Ges. Phys. Chem.* **1987**, *91*, 479.
(12) Wroblowa, Pan, Y. C.; Razumney, G. *J. Electroanal. Chem.* **1976**, *69*, 195.
(13) Anson, F. C. *J. Phys. Chem.* **1980**, *84*, 3336.

0022-3654/90/2094-7471$02.50/0